

High-inclination Centaur reservoirs beyond Neptune

F. Namouni

Université Côte d’Azur, CNRS, Observatoire de la Côte d’Azur, CS 34229, 06304 Nice, France
e-mail: namouni@oca.eu

Received 8 August 2025 / Accepted 30 October 2025

ABSTRACT

Context. Numerical simulations of the 4.5 Gyr past evolution of high-inclination Centaurs showed they originated from orbits beyond Neptune that were perpendicular to the Solar System’s invariable plane in a region called the polar corridor. The existence of the polar corridor is explained by the Tisserand inclination pathways followed by Neptune-crossing objects in the three-body problem. Recently, a study of Centaur injection in the three-body problem showed that Neptune-crossing transneptunian objects (TNOs) in the polar corridor with semi-major axes in the range [40:160] au have dynamical times that exceed the Solar System’s age suggesting the possible presence of long-lived reservoirs that produce high-inclination Centaurs.

Aims. We aim to demonstrate numerically the existence of such reservoirs in the Solar System by simulating the TNOs’ time-forward evolution under the gravitational perturbations of the giant planets, the Galactic tide and passing stars. We also aim to assess the efficiency of Centaur injection as a function of the initial inclination and determine if high-inclination Centaurs may be produced by low inclination reservoirs.

Methods. The motion of the giant planets, TNOs and passing stars is simulated using the IAS15 N -body numerical integrator of the REBOUND package. The Galactic tide is included using the REBOUNDx package. Two TNO orbit types are considered in the semi-major axis range [40:140] au: cold TNOs with circular orbits and hot TNOs with perihelion range [32:50] au. The TNOs Tisserand parameters T with respect to Neptune are taken in the range $-2 \leq T \leq 2.8$ corresponding to inclinations far from Neptune in the range $8^\circ \leq I_\infty \leq 135^\circ$ in order to examine Centaur injection at low and high initial inclinations.

Results. We find that TNO reservoirs in the semi-major axis range [50:140] au are long-lived and their populations peak at $T = 0.5$ and $T = -1.5$. Saturn is found to induce secondary structures in the polar corridor by holding the perihelia of a fraction of high-inclination reservoir material. We find that the Centaur inclination at minimum semi-major axis depends linearly on the Tisserand parameter regardless of the initial semi-major axis. Its amplitude shows that low inclination reservoirs such as the early protoplanetary disk are unlikely to produce high-inclination Centaurs in contrast to reservoirs in the polar corridor.

Conclusions. We identified the likely location of the closest reservoirs to Neptune populated by TNOs captured in the early Solar System that produce high-inclination Centaurs. The Legacy Survey of Space and Time of the Vera Rubin Observatory will be able to constrain the reservoirs’ extent and population size.

Key words. Celestial mechanics – Kuiper belt: general – Comets: general – Minor planets, asteroids: general

1. Introduction

Solar System Centaurs with inclinations larger than 60° are conventionally known as high-inclination Centaurs. Like low inclination Centaurs, they originate from planet-crossing orbits beyond Neptune but unlike low inclination Centaurs, their numbers cannot be explained by the protoplanetary disk in the early Solar System (Fernández et al. 2016; Fraser et al. 2022; Kaib & Volk 2022). High-resolution simulations of the past orbits of 19 real high-inclination Centaurs over 4.5 Gyr showed that they tend to be polar with respect to the Solar System’s invariable plane accumulating in the so-called polar corridor that extends beyond Neptune’s orbit (Namouni & Morais 2018, 2020) (hereafter Papers I and II). The polar corridor’s existence is rooted in the conservation of the Tisserand parameter of Neptune-crossing TNOs that ensures that their dynamical evolution follows Tisserand inclination pathways over Gyr-timescales regardless of whether time flows forward or backward (Namouni 2022) (hereafter Paper III).

The semi-major axis spread of -4.5 Gyr high-inclination Centaur clone orbits in the polar corridor extends from the scattered disk’s inner edge to the Oort cloud indicating a wide region of origin (Papers I and II). The Oort cloud, in particu-

lar, is a known possibility (Brasser et al. 2012b; Ito & Higuchi 2024). The presence of Oort cloud matter at -4.5 Gyr requires it to have been captured by the Solar System from the material in the stellar cluster of its birth (Fernández & Brunini 2000; Levison et al. 2010; Brasser et al. 2012b; Jílková et al. 2016; Hands et al. 2019; Kaib et al. 2019). Studies of the relaxation of the early flat protoplanetary disk through the orbital instability phase of the Solar System’s planets demonstrated that the Oort cloud formed through the scattering of disk matter later than -4.5 Gyr cannot explain the numbers of high-inclination Centaurs (Kaib et al. 2019; Nesvorný et al. 2019). Orbits of high-inclination Centaurs may be generated by hypothetical planets in the outer Solar System from an extended Kuiper belt (Batygin & Brown 2016; Lykawka & Ito 2023) but these models neglect the stellar environment of the Solar System known to induce instability over Gyr timescales (Kaib & Raymond 2025).

In this paper, we examine a new possible radial origin suggested by the semi-major axis spread of -4.5 Gyr high-inclination Centaur clone orbits in the polar corridor. The -4.5 Gyr semi-major axis probability distribution functions were found to peak outside Neptune’s orbit in the semi-major axis range [70:100] au (Paper II). These peaks may indicate a sta-

ble region where TNO reservoirs are currently present in the polar corridor and have been supplying high-inclination Centaurs to the giant planets' domain. As a first step in understanding the dynamical origin of the semi-major axis distribution peaks, we studied the dynamics of Neptune-crossing TNOs in the Sun-Neptune-TNO three-body problem (Namouni 2024) (hereafter Paper IV). This first step is important as the dynamics of Neptune-crossing TNOs is determined to a great extent by the conservation of the Tisserand parameter that gives rise to the concept of Tisserand inclination pathways. A Tisserand inclination pathway describes how orbital inclination evolves as Neptune is approached, and how the TNO is possibly injected as a Centaur before it eventually recedes from the planet to the outer Solar System if it does not experience collision or ejection. The Tisserand inclination pathway depends only on the TNO's Tisserand parameter and the planet's semi-major axis. In particular, it is independent of time. This makes the Tisserand parameter the perfect tool to probe original inclinations. The study of the TNO injection process in Paper IV, as a function of the Tisserand parameter, revealed the existence of a stable region in the polar corridor with semi-major axis range [40:160] au where the dynamical time of planet-crossing TNOs exceeds the Solar System's age suggesting the possible presence of long-lived Centaur-supplying TNO reservoirs. The fact that the stable region found in the three-body problem using time-forward integration is consistent with the -4.5 Gyr semi-major axis distribution peaks of Paper II obtained using time-backward integration in the presence of the four giant planets is encouraging. If the existence of this stable region is confirmed numerically in a comprehensive time-forward simulation of the Solar System, it will indicate the likely location of the closest reservoirs to Neptune populated by TNOs that were captured in the polar corridor 4.5 Gyr ago and that produce high-inclination Centaurs. In this paper, we provide such confirmation.

In Section 2, we describe the initial conditions used in this work and their relationship to the stable region found in Paper IV. In particular, parameter space is enlarged beyond the three-body stable region's Tisserand parameter range and beyond the perihelion range of the past orbits of high-inclination Centaurs of Papers I and II. In Section 3, we describe the simulation method used to follow the time-forward evolution of TNO reservoirs subject to the perturbations of the four giant planets, the Galactic tide and passing stars. The reservoirs' state at the simulation's end is discussed as a function of the initial semi-major axis and Tisserand parameter in Section 4. The reservoirs' stability is confirmed as well as Neptune's role in providing Tisserand inclination pathways for the reservoirs' material to follow. It is also found that Saturn produces secondary structures in the polar corridor as it retains a fraction of TNOs perihelia near its orbit. In Section 5, Centaur injection is described. In particular, the number of injected Centaurs is found to depend linearly on the Tisserand parameter. In Section 6, the features of Centaurs orbits are described. Additional linear relations with respect to the Tisserand parameter are found, for the Centaur minimum semi-major axis, for the Centaur perihelion at minimum semi-major axis and the Centaur inclination at minimum semi-major axis. The latter explains why high-inclination Centaurs are unlikely to be produced from low inclination reservoirs such as the early protoplanetary disk. Section 7 contains concluding remarks. In the remainder of this paper, The Tisserand parameter is specified with respect to Neptune unless stated otherwise.

2. Reservoirs' initial extent

We build the reservoirs' initial state using three results from the 4.5 Gyr time-backward numerical simulation of 19 real high-inclination Centaurs using ~ 20 million clones (Papers I and II). The first result is the Centaurs' past polar state. Starting with initial inclinations extending over $[62^\circ:173^\circ]$, the -4.5 Gyr end state inclinations extended over $[60^\circ:90^\circ]$ with a standard deviation $\sim 10^\circ$ beyond Neptune's orbit. An analytical analysis of the three-body problem (Paper III) demonstrated that this clustering is the manifestation of the Tisserand parameter's conservation that in turn makes Centaurs and TNOs follow the Tisserand inclination pathway:

$$I_{\text{Tiss}}(a, T, a_p) = \arccos \left(\left[T - \frac{a_p}{a} \right] \left[4 \left(2 - \frac{a_p}{a} \right) \right]^{-\frac{1}{2}} \right), \quad (1)$$

$$\text{where } T = \frac{a_p}{a_0} + 2 \left[\frac{a_0(1 - e_0^2)}{a_p} \right]^{\frac{1}{2}} \cos I_0, \quad (2)$$

e_0 and I_0 are the asteroid's initial eccentricity and inclination and a_0 ad a_p are the asteroid's and the planet's semimajor axes. The Tisserand inclination pathway is independent of time and perihelion and defines the polar corridor as the extent in aI -space between $I_{\text{Tiss}}(a, 2, a_p)$ and $I_{\text{Tiss}}(a, -1, a_p)$. This corresponds approximately to the inclination range of the -4.5 Gyr orbits of high-inclination Centaurs.

The second result is the extent of the -4.5 Gyr semi-major axis distributions peaks in the region [70:100] au. This extent is smaller than the three-body stable region (Paper IV), [40:160] au, where TNO dynamics was followed at Neptune's collision singularity. The discrepancy in the inner boundary has two reasons. First, the giant planets' perturbations are stronger at the inner edge of the three-body stable region. Secular perturbations from the giant planets, in particular, increase instability as they may raise significantly the eccentricity of planet-crossing and non-crossing TNOs. Second, the initial conditions at Neptune's singularity include, for a given Tisserand parameter, TNOs with small perihelia that would have crossed the unmodeled orbits of Jupiter, Saturn and Uranus and became unstable. In contrast, Papers I and II indicated that past high-inclination Centaur orbits in the polar corridor did not have arbitrary perihelia but they clustered mainly in the vicinity of Neptune's orbit. The discrepancy in the outer boundary is unclear. Despite the proximity of the 100 au boundary to the location of the outer 1:6 mean motion resonance with Neptune, it was shown in Paper IV that resonances do not fully explain the stability of high-inclination Neptune-crossing TNOs.

The Tisserand parameter range of the three-body stable region where the dynamical time exceeds 4.5 Gyr is $[-1:0]$ corresponding to an inclination far from Neptune $90^\circ \leq I_\infty \leq 110^\circ$ where I_∞ is given as (Paper III):

$$I_\infty(T) = \arccos(T / \sqrt{8}). \quad (3)$$

In Papers III and IV, we demonstrated that a TNO may be injected inside Neptune's orbit only if its Tisserand parameter $T \geq -1$. Once injected, its Centaur inclination becomes retrograde if $T \leq 2$ and remains prograde otherwise. The $T = -1$ limit is specific to the three-body problem and stems from the Tisserand inclination pathway. The pathway guides the TNO towards the planet up to a reflection semi-major axis that depends on T and Neptune's semi-major axis a_N given as:

$$a_{\text{refl}} = a_N [T - 2 + 2\sqrt{3 - T}]^{-1}. \quad (4)$$

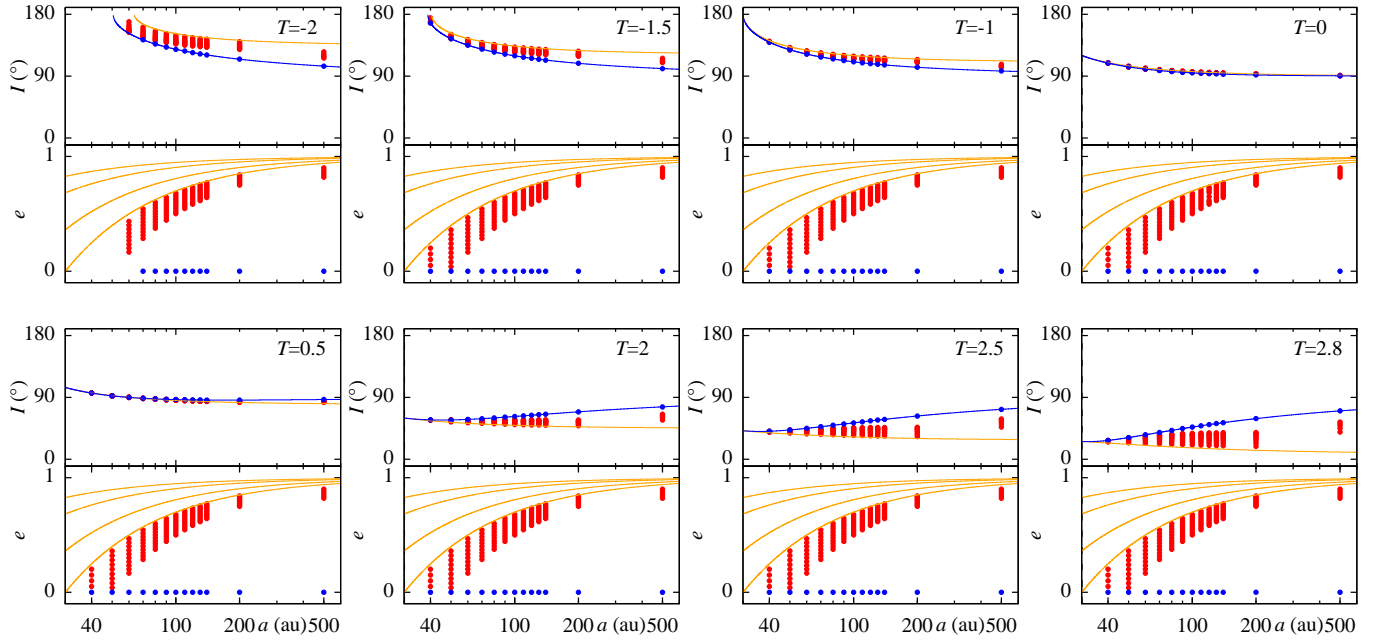


Fig. 1: Initial state of the TNO reservoirs for different Tisserand parameters T indicated in the top right corner of each panel. Hot TNOs are shown in red and cold TNOs are shown in blue. The solid orange and blue curves in the inclination panels are respectively the Tisserand inclination pathway (2) and the initial inclination of circular orbits (5). In the eccentricity panels, the curves indicate perihelia that match the four giant planets' semi-major axes.

The TNO then reverses its radial motion and moves away from the planet. The limit $T = -1$ is when reflection occurs at Neptune's semi-major axis. For $T < -1$, the TNO is reflected outside the planet's orbit and may not become a Centaur. The addition of Jupiter, Saturn and Neptune to the simulation modifies the three-body injection process and a larger T -range is necessary. The Tisserand parameter of a TNO that may cross a planet's orbit must satisfy $-\sqrt{8} \leq T \leq \sqrt{8} \sim 2.82$ (Paper III). To probe the transfer of prograde orbits to high-inclination retrograde orbits, the reservoirs' Tisserand parameter range is enlarged to $[-2:2.5]$ with a 0.5-step from the three-body problem stability range of $[-1:0]$. The additional value $T = 2.8$ ($I_{\infty} \sim 8^\circ$) was included to provide a means of comparison with low-inclination dynamics.

We examine two orbit types in the semi-major axis range [40:140] au with a 10 au-step: hot and cold TNOs. Hot TNOs are test particles with eccentric orbits and perihelia in the range [32:50] au with a 2 au-step¹. These reservoirs could be part of the material captured by the Solar System in its birth cluster. The perihelion range is based on the third result of the time-backward simulations that showed polar corridor orbits' perihelia clustered at Neptune's orbit. Enlarging the perihelion range beyond Neptune's semi-major axis explores whether the giant planets' combined perturbations produce high-inclination Centaurs from an initial population of non-planet-crossing TNOs.

Cold TNOs are test particles with circular orbits. These reservoirs have no plausible physical origin. They are used to assess how distant from Neptune can perihelia be before TNOs are no longer injected as Centaurs. Hot TNO ensembles with ($a = 200$ au and $32 \leq q(\text{au}) \leq 50$ and a 2 au q -step) and ($a = 500$ au, $50 \leq q(\text{au}) \leq 90$ and a 10 au q -step) along with cold ensembles at the same semi-major axes were also simulated to characterize the dynamics far from the reservoirs.

For each set (a, T, q) , 100 orbits are generated by drawing the orbital angles, mean longitude, longitude of ascending node and argument of perihelion, from a uniform distribution. As the Tisserand inclination pathway is independent of any angles, the 100 orbits may evolve on the same pathway in the three-body problem. Furthermore, regardless of the initial a and q , ensembles with the same T value may evolve on the same Tisserand inclination pathway.

Figure 1 shows the reservoirs' initial extent as a function of eccentricity, inclination and semi-major axis for $T = -2, -1.5, -1, 0, 0.5, 2, 2.5$ and 2.8 . Hot and cold TNOs are shown in red and blue respectively. Larger perihelia imply larger (smaller) inclinations than the Tisserand pathway's for (retrograde) prograde motion. This deviation from the inclination pathway increases with the initial semi-major axis and has a limit value, I_{circ} , for circular orbits given as:

$$I_{\text{circ}}(a, T, a_N) = \arccos \left(\left[T - \frac{a_N}{a} \right] \left[\frac{4a}{a_N} \right]^{-\frac{1}{2}} \right), \quad (5)$$

and shown in the inclination panels of Figure 1 as the blue curve along with the Tisserand inclination pathway (2) as the orange curve.

3. Simulation method

Dynamical evolution is simulated 4.5 Gyr forward in time using the IAS15 N -body integrator of the REBOUND package (Everhart 1985; Rein & Spiegel 2015; Rein & Tamayo 2017). The simulations include the four giant planets, the TNO ensembles and passing stars. The terrestrial planets' mass was added to the Sun's. The three-dimensional Galactic tide (Heisler & Tremaine 1986) and relative inclination of the ecliptic and Galactic planes were included using the REBOUNDx

¹ For $a = 40$ au, $32 \text{ au} \leq q \leq 38$ au

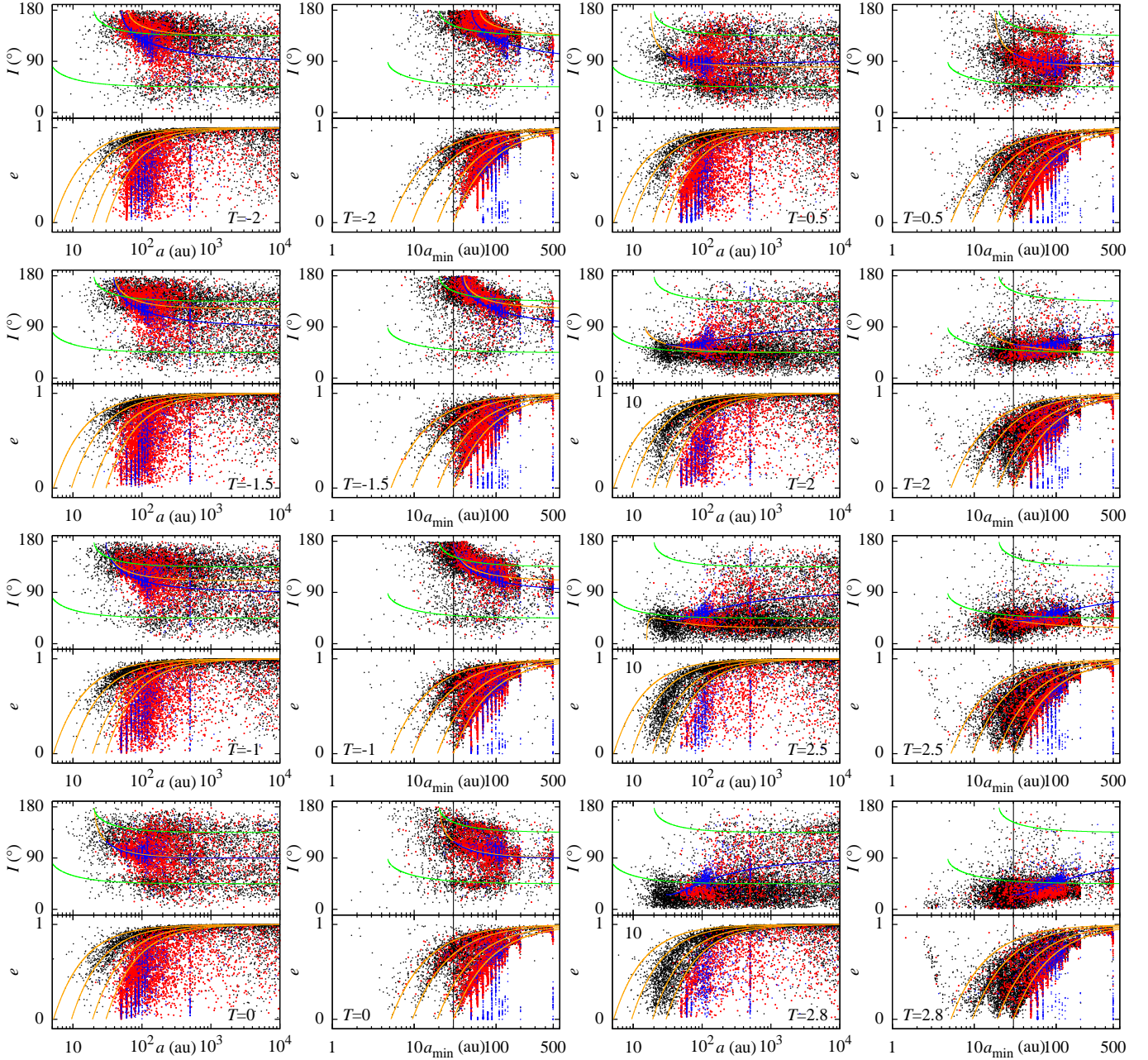


Fig. 2: TNO reservoirs at 4.5 Gyr for different Tisserand parameters T . Hot TNOs are shown in red and cold TNOs are shown in blue. Unstable TNOs are shown in black at the last sampling epoch before instability. The first and third columns display the orbital distributions in the (a, I) and (a, e) planes. The second and fourth columns show I , e and a at minimum semimajor axis where a vertical black line denotes Neptune's semi-major axis. The solid orange and blue curves in the inclination panels are respectively the Tisserand inclination pathway $I_{\text{Tiss}}(a, T, a_N)$ (2) and the circular orbits' initial inclination $I_{\text{circ}}(a, T, a_N)$ (5) with respect to Neptune. The solid green curves for retrograde and prograde inclinations respectively are the Tisserand inclinations pathways with respect to Saturn $I_{\text{Tiss}}(a, -2, a_S)$ (135° inclination) and $I_{\text{Tiss}}(a, 2, a_S)$ (45° inclination). In the eccentricity panels, the curves indicate perihelia that match the four giant planets' semi-major axes. The Tisserand inclination pathway with respect to Neptune is not shown for $T = 2.8$ because the expression (2) is not valid for $T > 2.7$ (see Paper III for details).

package (Tamayo et al. 2020). The Oort constants, $A = 15.3 \text{ km s}^{-1} \text{ kpc}^{-1}$, $B = 11.9 \text{ km s}^{-1} \text{ kpc}^{-1}$, and star density in the solar neighbourhood, $\rho_0 = 0.119 M_\odot \text{ pc}^{-3}$, were obtained from Gaia's first data release (Bovy 2017; Widmark & Monari 2019) and were used in Papers I and II.

The list of passing stars was generated using the algorithm of (Heisler et al. 1987) and the stellar categories of Rickman et al. (2008) and their corresponding statistics (García-Sánchez et al.

2001). The 66 230 passing stars are introduced in the simulation according to their Solar System's encounter epoch. Their evolution is integrated within 1 pc from the Solar System. Multiple stars may be present in the simulation at the same time and therefore interact with one another. The star residency time within 1 pc measured over 4.5 Gyr is $20 \text{ kyr} \pm 13 \text{ kyr}$ with a maximum value of 415 kyr.

achieved over 4.5 Gyr and the corresponding eccentricities and inclinations for all orbital types stable and unstable.

The reservoirs' semi-major axis extent is similar to the initial state's. TNOs scattered by the combined effects of the giant planets, Galactic tide and passing stars are also present far outside the reservoirs' domain. Secular perturbations cause a larger dispersion in eccentricity and inclination for hot TNOs. Cold TNOs remain mainly with low eccentricity orbits as evidenced by their clustering along the inclination curve of circular orbits (5). As the Tisserand parameter increases toward the polar corridor boundary's $T = 2$, instability is greater and the reservoirs are depleted. Examination of the minimum semi-major axis distributions shows that starting from $T = -2$ minimum perihelia are distributed between Saturn and Neptune but the perihelion range narrows around Neptune's orbit outside the polar corridor as T increases and initial inclinations get smaller.

The Tisserand inclination pathways with respect to Neptune for the bulk of the reservoirs' material are generally followed for all values of the Tisserand parameter. The pathways are shown in orange in the inclination panels of Figure 2. A novel process related to Saturn adds secondary inclination pathways that are present for $T \leq 2$ and prominent inside the polar corridor. Saturn appears to retain a small fraction of reservoir material with perihelia at Saturn's orbit whereas their orbits are pushed back outside Neptune's. This material follows two specific Tisserand inclination pathways with respect to Saturn regardless of the initial Tisserand parameter, T . These are $I_{\text{Tiss}}(a, -2, a_S)$ and $I_{\text{Tiss}}(a, 2, a_S)$ (2) where a_S is Saturn's semi-major axis. The pathways correspond to inclinations far from Neptune $I_\infty = 135^\circ$ and $I_\infty = 45^\circ$ (3) and appear as the green curves in the inclination panels of Figure 2. These secondary populations are prominent for $T = 0$ and $T = 0.5$ in Figure 2 and their density decreases outside the polar corridor as T tends to -2 . Investigating Saturn's secondary inclination pathways is beyond the scope of this paper.

Figure 3 shows the ratio of the number of surviving hot TNOs to their initial number, denoted f_{TNO} , for different initial semi-major axes as a function of the Tisserand parameter. For each semi-major axis, all the different perihelia are included in the statistic – the perihelion dependence is discussed in the next section. Four semi-major axis groups are visible. First, TNOs with initial a in the range $[70:100]$ au follow a similar distribution to that of the dynamical time in the three-body problem found in Paper IV (Figure 7 therein). The dynamical time may be considered a proxy for f_{TNO} . The three-body dynamical time versus Tisserand parameter, has three peaks: a prominent one near $T \sim -0.7$, a moderate one near $T \sim 0.8$ and a smaller one near $T \sim 2.2$. The 6-body plus passing stars configuration of the present framework displaces the three peaks to $T \sim -1.5$ with $f_{\text{TNO}} \sim 60\%$ for $a = 80$ au, to $T \sim 0.5$ with $f_{\text{TNO}} \sim 50\%$ for $a = 70$ au and to $T \sim 2$ with $f_{\text{TNO}} \sim 30\%$ for $a = 100$ au. This group's range of $[70:100]$ au is reminiscent of the semi-major axis probability distributions peaks discussed in Sections 1 and 2.

The ensembles with $a = 50$ au and $a = 60$ au form the second group whose retrograde peak has been all but erased in favor a prominent peak at $T = 0.5$ and $f_{\text{TNO}} \sim 60\%$ for $a = 60$ au. The third group has a semi-major axis range $[110:140]$ au whose f_{TNO} decrease steadily with increasing T . The fourth group is made up of the ensembles of $a = 40$ au, $a = 200$ au and 500 au that are mainly unstable confirming the existence of two stability boundaries, an inner one between 40 au and 50 au and an outer one between 140 au and 200 au.

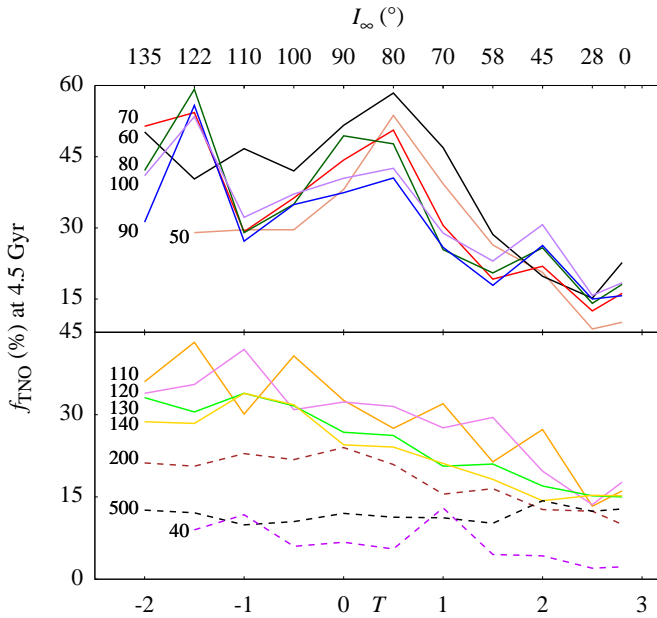


Fig. 3: Fraction of hot TNOs that survived 4.5 Gyr as a function of the Tisserand parameter T (and I_∞) for semi-major axes $50 \leq a(\text{au}) \leq 100$ (top panel) and $110 \leq a(\text{au}) \leq 500$ along with $a = 40$ au (bottom panel). The number next to each curve is the initial semi-major axis.

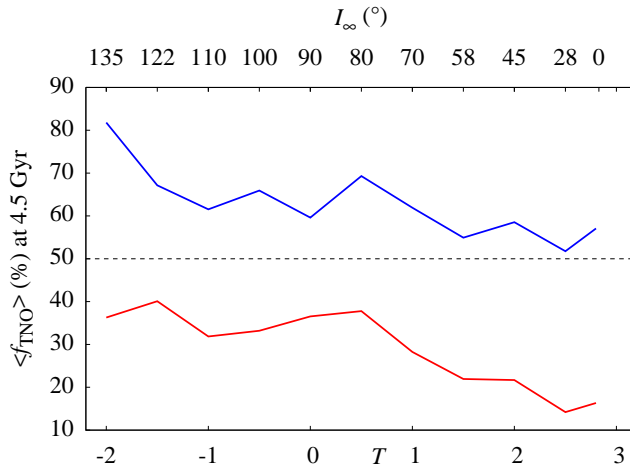


Fig. 4: Average fraction of cold TNOs (in blue) and hot TNOs (in red) that survived 4.5 Gyr as a function of the Tisserand parameter T (and I_∞).

The orbits of 142 500 TNOs were integrated and their minimum semi-major axes monitored throughout the simulation. TNOs are removed from the simulation in case of collision or ejection.

4. Reservoirs' state at 4.5 Gyr

The end states of the TNO reservoirs in the Ia - and ea -planes are shown in Figure 2 for the Tisserand parameters, $T = -2, -1.5, -1, 0, 0.5, 2, 2.5$ and 2.8 (as in Figure 1). Hot TNOs are shown in red and cold TNOs in blue. Unstable orbits are shown in black at the last sampled epoch before instability. Also shown are the TNOs' distributions of minimum semi-major axes

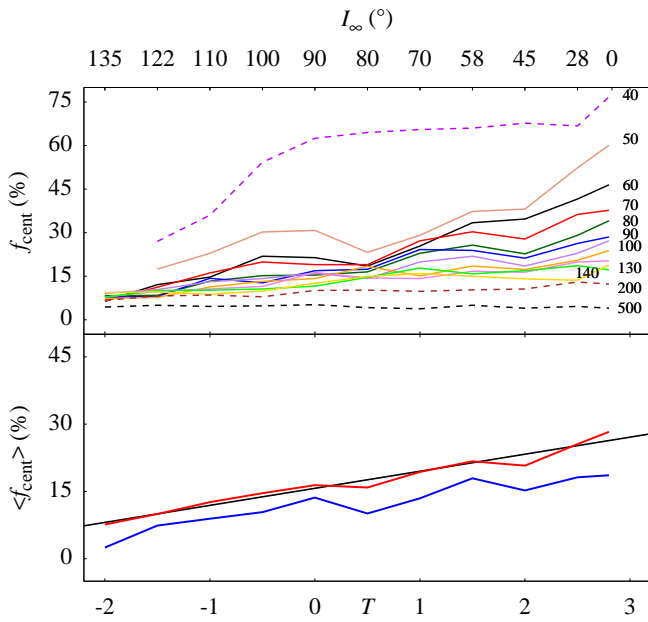


Fig. 5: Fraction of hot TNOs that became Centaurs as a function of the Tisserand parameter T (and I_∞). In the top panel, f_{cent} corresponds to the initial semi-major axis given next to each curve. In the bottom panel, the semi-major axis-averaged, $\langle f_{\text{cent}} \rangle$, of initially cold and hot TNOs are shown in blue and red respectively. The black line is $\langle f_{\text{cent}} \rangle(\%) = 17 + 4.3T$.

The values of f_{TNO} in the range [50:140] au confirm that TNO reservoirs are long-lived in the presence of all giant planets, passing stars and the Galactic tide. In particular, the peaks at $I_\infty = 122^\circ$ ($T = -1.5$) and $I_\infty = 80^\circ$ ($T = 0.5$) single out inclinations that have the largest current populations. The average of f_{TNO} over all semi-major axes for hot and cold TNOs, denoted $\langle f_{\text{TNO}} \rangle$, is shown a function of the Tisserand parameter in Figure 4. It indicates that cold TNOs on average have a 4.5 Gyr dynamical time as $\langle f_{\text{TNO}} \rangle > 50\%$ unsurprisingly since they mainly retain low eccentricity orbits. Hot TNOs fractions decrease with T peaking at $T \sim -1.5$ with $\langle f_{\text{TNO}} \rangle \sim 40\%$, $T \sim 0.5$ with $\langle f_{\text{TNO}} \rangle \sim 35\%$ and $T \sim 2$ with $\langle f_{\text{TNO}} \rangle \sim 22\%$.

5. Centaur injection

The ratio of the number of TNOs whose semi-major axes became smaller than Neptune's over 4.5 Gyr, to the initial TNO number is denoted $f_{\text{cent}}(a, T)$. The initial TNO number of each semi-major axis includes the full perihelion range and the Centaur number includes stable and unstable orbits. The top panel of Figure 5 shows $f_{\text{cent}}(a, T)$ for hot TNOs and different semi-major axes as a function of the Tisserand parameter. The Centaur fraction increases with the Tisserand parameter at a larger rate as the semi-major axis is closer to Neptune. TNOs with low to moderate inclination are injected in greater numbers than high-inclination TNOs as their corresponding reservoirs are depleted because of instability. The hot TNO ensembles with $a = 200$ au and 500 au contribute smaller Centaur numbers also because of instability. On the other hand, instability for TNOs with $a = 40$ au translates into the largest injection rate because of its proximity to Neptune. For Tisserand parameters $T < -1$, Centaur fraction is finite indicating that the presence of the giant planets and passing stars breaks Neptune's reflecting ability that

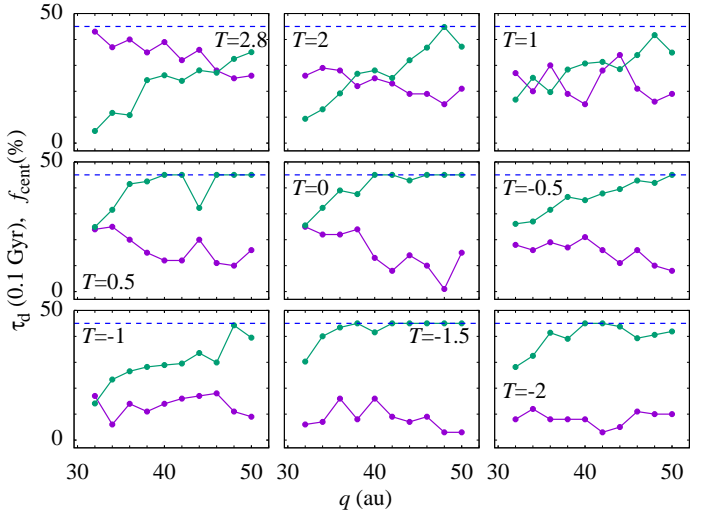


Fig. 6: Dynamical time (green) and Centaur fraction (purple) for initially hot TNOs with an initial $a = 80$ au as a function of perihelion for different Tisserand parameters. The dashed blue line is $\tau_d = 4.5$ Gyr.

was evidenced in the three-body problem with the existence of a_{refl} (4) (Papers III and IV) – further evidence is given in the next section.

We define $\langle f_{\text{cent}} \rangle$ as the semi-major axis averaged Centaur fraction in the stable region. The TNO ensembles of $a = 40$ au, 200 au and 500 au are excluded from the hot TNO statistics because they lie outside the stability region. This will be applied in the remainder of the paper when averaging over semi-major axes. The bottom panel of Figure 5 shows that $\langle f_{\text{cent}} \rangle$ of hot and cold TNOs are remarkably similar. The hot TNO $\langle f_{\text{cent}} \rangle$ follows a simple linear expression that depends on the Tisserand parameter as follows $\langle f_{\text{cent}} \rangle(\%) = 17 + 4.3T$.

More information on the injection process is found by examining the dependence of the Centaur number on perihelion for hot TNOs and on semi-major axis for cold TNOs. Figure 6 shows non-averaged $f_{\text{cent}}(a, T, q)$ along with the corresponding dynamical time, $\tau_d(a, T, q)$, for the ensembles with an initial $a = 80$ au. As stated in the Section 2, each (a, T, q) ensemble has 100 TNOs and $f_{\text{cent}}(a, T, q)$ is the fraction of those among them that became Centaurs. An ensemble's dynamical time is its median lifetime. It is meant as a stability indicator and not a dynamical time in the classical sense which is associated with a single orbit and derived from its clones' evolution. As such the TNOs' dynamical time, τ_d , shown here is an average of the classical dynamical times of the orbits that make up the (a, T, q) ensemble. It is found unsurprisingly that Centaur injection tends to increase with smaller perihelia for low to moderate inclinations ($T = 2.8$). However, the perihelion dependence become shallower for reservoirs inside the polar corridor ($-1 \leq T \leq 2$) suggesting that it is secular perturbations and not the initial perihelion that control Centaur injection – see the panel of $T = 1$. The dynamical time is an increasing function of perihelion and reaches 4.5 Gyr in the polar corridor and for $T > -1$. Its dependence on the Tisserand parameter inside the polar corridor is unclear but could be depend on the vicinity of T to the boundaries $T = -1$ and $T = 2$. Different initial semi-major axes of hot TNOs in the region [50:140] au have similar $f_{\text{cent}}(a, T, q)$ and dynamical times as a function of perihelion. The median and maximum dynamical times for the different perihelia respectively are 3 Gyr and 4.5 Gyr with the latter achieved in the polar corridor. The median and maximum

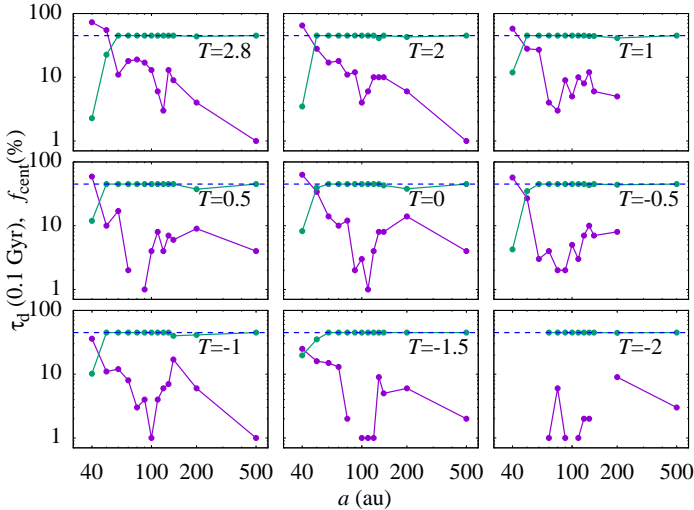


Fig. 7: Dynamical time (green) and Centaur fraction (purple) for initially cold TNOs as a function of semi-major axis for different Tisserand parameters. The dashed blue line is $\tau_d = 4.5$ Gyr. The empty semi-major axis ranges indicate absence of Centaur injection.

dynamical times are 2.4 Gyr and 3.5 Gyr for $a = 200$ au and 500 au, whereas for $a = 40$ au, they are 0.48 Gyr and 1.5 Gyr.

The Centaur fraction, $f_{\text{cent}}(a, T, q)$, and dynamical time of cold TNOs, $\tau_d(a, T, q)$, are shown in Figure 7. The number of injected Centaurs decreases exponentially with semi-major axis so that most injected Centaurs come for the smallest semi-major axes. This is visible on the dynamical times as they reach 4.5 Gyr as soon as $a \geq 60$ au regardless of the Tisserand parameter. It is interesting that regardless of which semi-major axis and perihelion contributes most to Centaur injection, the average Centaur fractions, $\langle f_{\text{cent}} \rangle$, of both hot and cold reservoirs are similar (Figure 5 bottom panel). Understanding this similarity's origin may uncover the common dynamical process underlying Centaur injection.

6. Injected Centaur orbits

The analysis of orbit injection in the three-body problem indicates that a Centaur orbit acquires its largest inclination at its minimum semi-major axis as it follows its Tisserand inclination pathway inside the planet's orbit (Paper III). This makes the inclination at minimum semi-major axis a useful diagnostic tool to access pre-injection original inclinations far from the planet (3) through the Tisserand parameter.

Figure 8 shows the Centaurs' inclination at minimum semi-major axis as a function of the Tisserand parameter for hot TNO reservoirs and the different initial semi-major axes. The statistics for an initial semi-major axis include all initial perihelia. The top panel displays the mean inclinations and the bottom panel the standard deviations. The dashed curves are those of $a = 40$ au (magenta), $a = 200$ au (brown) and $a = 500$ au (black) that lie outside the stable region. The remaining semi-major axes are not identified in the figure because the curves are close but generally from top to bottom the curves represent increasing semi-major axes. The color codes are those of Figures 3 and 5.

The mean inclinations remarkably share the same functional dependence on the Tisserand parameter regardless of semi-major axis. There is a Tisserand value around $T \sim -0.5$, for each semi-major axis, below which the mean inclination is constant and

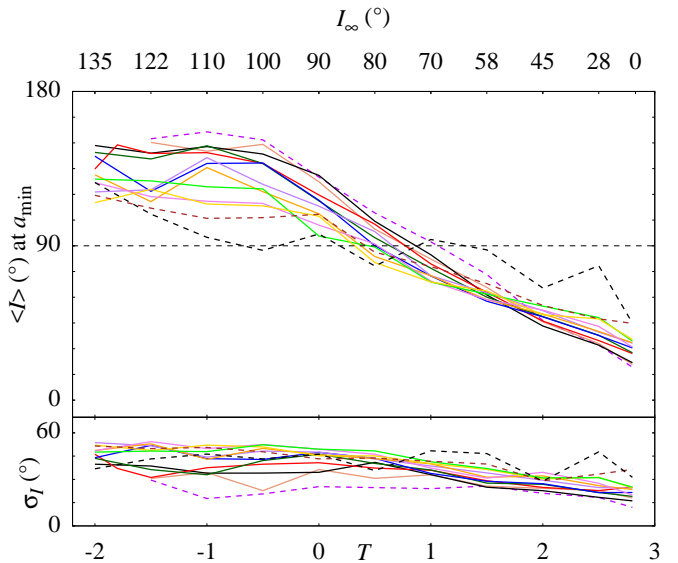


Fig. 8: Centaur inclination at minimum semi-major axis of initially hot TNOs as a function of the Tisserand parameter T (and I_∞) for semi-major axes $50 \leq a$ (au) ≤ 140 (solid curves) and $a = 40$ au (dashed magenta curve), $a = 200$ au (dashed black curve) and $a = 500$ au (dashed brown curve). The average inclination, $\langle I \rangle$, and standard deviation, σ_I , are shown in the top and bottom panels respectively.

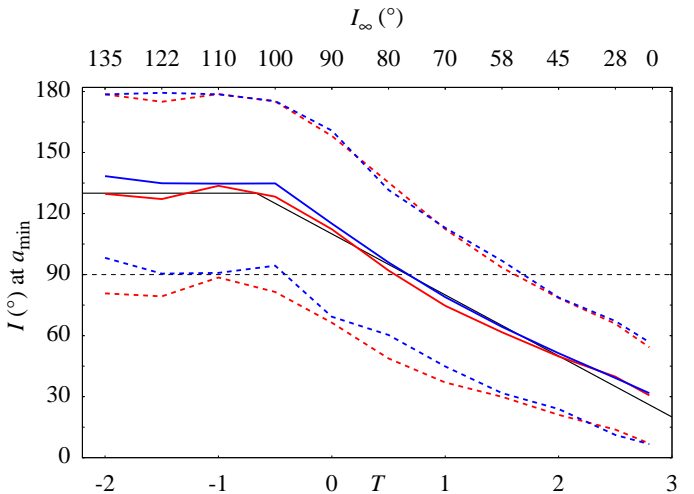


Fig. 9: Semi-major axis-averaged Centaur inclination at minimum semi-major axis of cold TNOs (blue) and hot TNOs (red) as a function of the Tisserand parameter T (and I_∞). Dashed blue and red lines are the corresponding standard deviations. The solid black lines are $\langle I \rangle = 110^\circ - 30^\circ T$ for $T \geq -0.67$ and $\langle I \rangle = 135^\circ$ otherwise.

beyond which inclination decreases linearly with the Tisserand parameter. The constant inclination value for $T < -0.5$ decreases from $\sim 150^\circ$ for 40 au to $\sim 120^\circ$ for 140 au.

Figure 9 shows the semi-major axis-averaged inclinations at minimum semi-major axis of Centaurs originating in the stable region as a function of the Tisserand parameter for hot and cold TNO reservoirs along with their standard deviations. The initially hot TNO Centaur-inclination is approximated by $\langle I \rangle = 110^\circ - 30^\circ T$ for $T \geq -0.67$ and $\langle I \rangle = 135^\circ$ otherwise. The

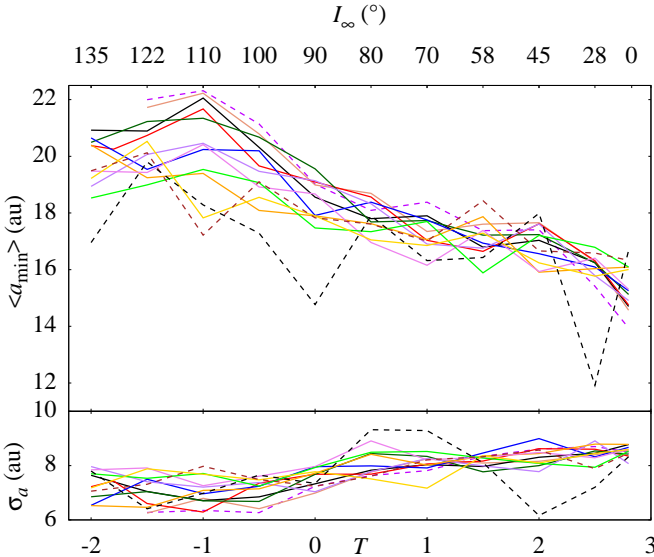


Fig. 10: Centaur minimum semi-major axis of initially hot TNOs as a function of the Tisserand parameter T (and I_∞) for semi-major axes $50 \leq a$ (au) ≤ 140 (solid lines) and $a = 40$ au (dashed magenta curve), $a = 200$ au (dashed brown line) and $a = 500$ au (dashed black line). The average semi-major axis, $\langle a_{\min} \rangle$, and standard deviation, σ_a , are shown in the top and bottom panels respectively.

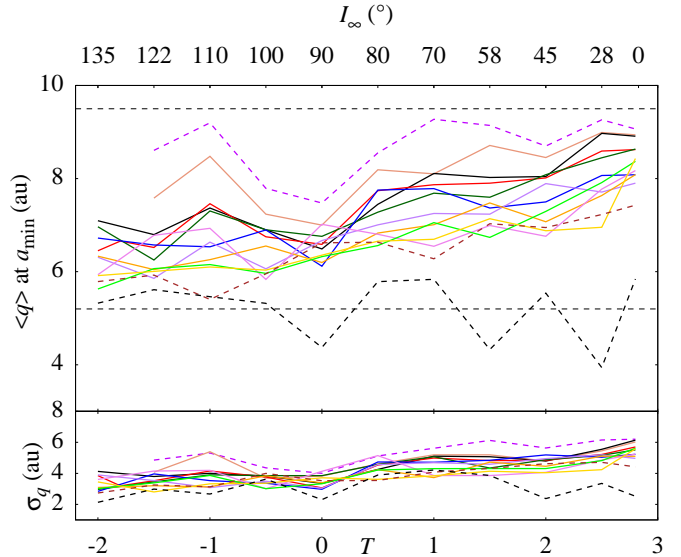


Fig. 12: Centaur perihelion at minimum semi-major axis of initially hot TNOs as a function of the Tisserand parameter T (and I_∞) for semi-major axes $50 \leq a$ (au) ≤ 140 (solid lines) and $a = 40$ au (dashed magenta curve), $a = 200$ au (dashed brown line) and $a = 500$ au (dashed black line). The average semi-major axis, $\langle q \rangle$, and standard deviation, σ_q , are shown in the top and bottom panels respectively.

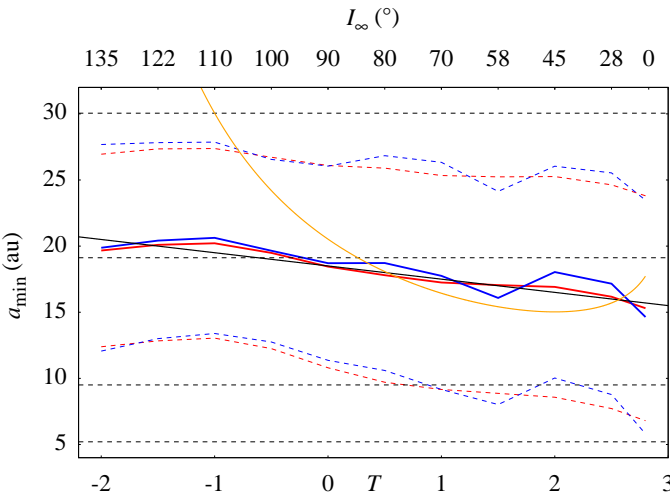


Fig. 11: Average Centaur minimum semi-major axis of cold TNOs (blue) and hot TNOs (red) as a function of the Tisserand parameter T (and I_∞). Dashed blue and red curves are the corresponding standard deviations. The solid black line is $\langle a_{\min} \rangle$ (au) = $18.5 - T$. The solid orange curve is the three-body reflection semi-major axis of Neptune (4). The planets' positions are indicated with dashed black lines.

cold TNO Centaur-inclination has a similar dependence. The inclination standard deviation increases steadily from $\sigma_I \sim 25^\circ$ at $T = 2.8$ to $\sigma_I \sim 45^\circ$ for $T = -2$.

The Centaur inclination at minimum semi-major axis shows that high-inclination Centaurs may not be produced by reservoirs with arbitrary initial inclinations. For instance, a low inclination reservoir with $T = 2.8$ has $\langle I \rangle \sim 30^\circ$. Retrograde Centaurs with inclinations 100° and 155° respectively lie at $3\sigma_I$ and $5\sigma_I$ from

the mean value. This explains the inability of relaxation models of the early planar protoplanetary disk to account for the numbers of high-inclination Centaurs. On the other hand, reservoirs in the polar corridor may produce polar and retrograde inclination Centaurs with statistical significance.

The minimum semi-major axes (mean and standard deviation) of hot TNOs, that achieved a Centaur orbit are shown in Figure 10 as a function of the Tisserand parameter for different initial semi-major axes. The minimum semi-major axis is averaged over all initial perihelia. The semi-major axes are not indicated because the curves are close. Centaur injection occurs across all values of the Tisserand parameter in contrast to the dynamics of the three-body problem. The minimum semi-major axes decrease with increasing T in a similar fashion. The large variations of the TNO ensembles with an initial $a = 500$ au comes for the small statistics of injected Centaurs. The minimum semi-major axes averaged over the different initial semi-major axes of Centaurs originating in the stable region are shown in Figure 11 for hot and cold TNOs. The two curves are similar and may be approximated by the linear expression $\langle a_{\min} \rangle$ (au) = $18.5 - T$ with a mostly constant standard deviation $\sigma_a \sim 8$ au. The three-body reflection semi-major axis of Neptune (4) shown in Figure 11 is of the same order as $\langle a_{\min} \rangle$ for $T > 0.4$ only as it does not account for the presence of the giant planets.

The perihelia at minimum semi-major axis (mean and standard deviation) of hot TNOs that achieved a Centaur orbit are shown in Figure 12 as a function of the Tisserand parameter for different initial semi-major axes. Mean perihelia and their standard deviations increase with increasing Tisserand parameter (decreasing initial inclination). It is also found that perihelia decrease with increasing initial semi-major axis. In particular, hot TNOs with $a = 500$ au are injected as Centaurs with perihelia around Jupiter's orbit. The semi-major axis averaged Centaur perihelia originating in the stable region are shown in Fig-

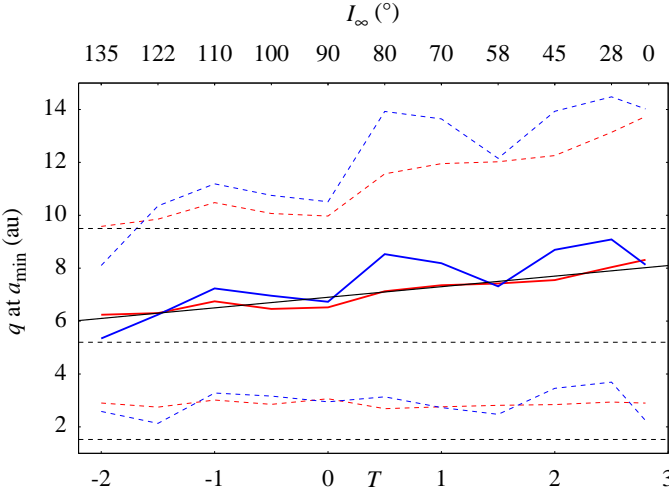


Fig. 13: Average Centaur perihelion at minimum semi-major axis of cold TNOs (blue) and hot TNOs (red) as a function of the Tisserand parameter T (and I_∞). Dashed blue and red curves are the corresponding standard deviations. The solid black line is $\langle q \rangle(\text{au}) = 6.9 + 0.4T$. The planets' positions are indicated with dashed black lines.

Figure 13. The hot TNO's mean perihelion as a function of the Tisserand parameter follows the linear relation $\langle q \rangle(\text{au}) = 6.9 + 0.4T$. The standard deviation increases from 3 au at $T = -2$ to 4 au at $T = 2.8$.

7. Conclusion

We set out to confirm the possible existence of current TNO reservoirs beyond Neptune's orbit that supply high-inclination Centaurs to the inner Solar System. This confirmation is based on simulating the gravitational perturbations of TNO reservoirs by the four giant planets, passing stars and the Galactic tide. The initial extent of the TNO reservoirs made use of two previous results. The first is the existence of a stable region in the semi-major range axis [40:160] au in the Sun-Neptune-TNO three-body problem (Paper IV). The second result is the proximity of past Centaur perihelia to Neptune's orbit found in the 4.5 Gyr time-backward simulations of 19 real high-inclination Centaurs using 20 million clones (Papers I and II). These extents were enlarged to better understand Centaur injection. The perihelion range was enlarged to [32:50] au, and a cold population with circular orbits was added to examine if Centaur injection is strongly dependent on perihelion. The Tisserand range was enlarged to [-2:2.8] or equivalently to TNO inclinations far from Neptune in the range [8°:135°] to examine Centaur injection beyond the polar corridor's retrograde inclination boundary in the Sun-Neptune-TNO three-body problem, $I_\infty \sim 110^\circ$ ($T = -1$), and also at low inclinations $I_\infty \sim 8^\circ$ ($T = 2.8$) of relevance to the relaxation of the early protoplanetary disk.

The numerical simulations confirmed the existence of current TNO reservoirs that provide high-inclination Centaurs to the Solar System as $\sim 40\%$ of the initial hot TNOs in the polar corridor survive 4.5 Gyr (Figure 4) in the semi-major axis range [50:140] au. It was also found that two specific Tisserand parameter values $T = 0.5$ and $T = -1.5$ (initial inclinations at infinity 80° and 122°) have the largest current populations (Figure 3). A finer analysis unveiled regions in perihelion space where the dynamical time is 4.5 Gyr and hence surviving hot TNOs constitute more than half the original reservoir (Figure 6).

The role of the Tisserand inclination pathway with respect to Neptune in the reservoirs' evolution is confirmed (Figure 2). The presence of all the giant planets modifies the polar corridor's structure as Saturn becomes the main perturber of a fraction of TNO material adding secondary Tisserand inclination pathways to the polar corridor (Figure 2). These pathways are defined only by Saturn regardless of the TNOs' initial Tisserand parameters. Neptune's reflection ability of incoming TNOs is also modified by the the giant planets as Centaur injection occurs outside the polar corridor's high-inclination boundary of $T = -1$. Although the presence of more planets may cause significant departures from three-body predictions, the Tisserand inclination pathway concept is robust as TNO dynamics remain based on it.

The existence of linear relations with respect to the Tisserand parameter that describe, the number of injected Centaurs (Figure 5), the Centaur inclination at minimum semi-major axis (Figure 9) and the Centaur minimum semi-major axis (Figure 11), affirms the role of the Tisserand parameter as the main control parameter in TNO dynamics. These relations were obtained by averaging over initial perihelia and semi-major axes for hot and cold TNOs. That the two populations follow similar Tisserand parameter-based linear relations indicates that the Centaur injection process is largely independent of the initial perihelia. The dependence of the mean Centaur perihelia on the initial semi-major axis showed the larger the TNO initial semi-major axis, the smaller the perihelion (Figure 12). Beyond this characterization of the injected Centaur orbits of high-inclination-TNO reservoirs, the linear relations will help discriminate between different high-inclination Centaur origins such as the Oort cloud component formed by the protoplanetary disk and the excitation caused by additional planets beyond Neptune provided that Centaur injection is analyzed in terms of the Tisserand parameter using orbital elements at minimum semi-major axis.

The most compelling result regarding Centaur injection is perhaps how the Centaur inclination at minimum semi-major axis depends on the Tisserand parameter and how it is independent of the initial semi-major axis (Figure 8). It explains why high-inclination Centaurs may not be produced with statistical significance from a low inclination reservoir such as the early protoplanetary disk, and why matter in the polar corridor may yield Centaurs with retrograde orbits.

Matter in the stable region at -4.5 Gyr is unlikely to originate in the early planetesimal disk because it was flat and did not extend beyond ~ 30 au in order to explain Neptune's current location (Gomes et al. 2004). The natural source for that matter is the stellar environment of the early Solar System. Simulations of interstellar matter capture in the Sun's birth cluster form the inner Oort cloud with an inner edge near 100 au (Brasser et al. 2012a) which falls in the middle of the stable region found in this work. Simulations of star encounters in the presence of protoplanetary disks show that it is possible to capture planetesimals at high inclination while preserving a star's flat planetesimal disk (Hands et al. 2019). After matter exchange in the Solar System's early environment has settled, the stable region of this work is where the TNO reservoirs may currently be found nearest to the giant planets. In similar way to the Trojans asteroids found at Jupiter's stable Lagrange points that are relics of early planet formation, the high-inclination reservoirs are relics of the Solar System's interactions with the stars of its birth cluster. The Legacy Survey of Space and Time (LSST) of the Vera Rubin Observatory will be able to constrain their extent and population size through its coverage of high ecliptic latitudes necessary to detect eccentric polar TNOs that spend more time above the ecliptic plane (Kurlander et al. 2025).

Acknowledgements. The author thanks the reviewer for their comments. The simulations in this work were performed using HPC resources of the National Facility GENCI-CINES (Grants 2024-AD010415952 and 2025-AD010416591) and on the SIGAMM Cluster hosted at the Observatoire de la Côte d’Azur.

References

Batygin, K. & Brown, M. E. 2016, *ApJ*, 833, L3
 Bovy, J. 2017, *MNRAS*, 468, L63
 Brasser, R., Duncan, M. J., Levison, H. F., Schwamb, M. E., & Brown, M. E. 2012a, *Icarus*, 217, 1
 Brasser, R., Schwamb, M. E., Lykawka, P. S., & Gomes, R. S. 2012b, *MNRAS*, 420, 3396
 Everhart, E. 1985, in *Astrophysics and Space Science Library*, Vol. 115, IAU Colloq. 83: Dynamics of Comets: Their Origin and Evolution, ed. A. Carusi & G. B. Valsecchi, 185
 Fernández, J. A. & Brunini, A. 2000, *Icarus*, 145, 580
 Fernández, J. A., Gallardo, T., & Young, J. D. 2016, *MNRAS*, 461, 3075
 Fraser, W. C., Dones, L., Volk, K., Womack, M., & Nesvorný, D. 2022, arXiv e-prints, arXiv:2210.16354
 García-Sánchez, J., Weissman, P. R., Preston, R. A., et al. 2001, *A&A*, 379, 634
 Gomes, R. S., Morbidelli, A., & Levison, H. F. 2004, *Icarus*, 170, 492
 Hands, T. O., Dehnen, W., Gration, A., Stadel, J., & Moore, B. 2019, *MNRAS*, 419, 1064
 Heisler, J. & Tremaine, S. 1986, *Icarus*, 65, 13
 Heisler, J., Tremaine, S., & Alcock, C. 1987, *Icarus*, 70, 269
 Ito, T. & Higuchi, A. 2024, *Planet. Space Sci.*, 253, 105984
 Jílková, L., Hamers, A. S., Hammer, M., & Portegies Zwart, S. 2016, *MNRAS*, 457, 4218
 Kaib, N. A., Pike, R., Lawler, S., et al. 2019, *AJ*, 158, 43
 Kaib, N. A. & Raymond, S. N. 2025, *Icarus*, 439, 116632
 Kaib, N. A. & Volk, K. 2022, arXiv e-prints, arXiv:2206.00010
 Kurlander, J. A., Bernardinelli, P. H., Schwamb, M. E., et al. 2025, *AJ*, 170, 99
 Levison, H. F., Duncan, M. J., Brasser, R., & Kaufmann, D. E. 2010, *Science*, 329, 187
 Lykawka, P. S. & Ito, T. 2023, *AJ*, 166, 118
 Namouni, F. 2022, *MNRAS*, 510, 276 (Paper III)
 Namouni, F. 2024, *MNRAS*, 527, 4889 (Paper IV)
 Namouni, F. & Morais, M. H. M. 2018, *MNRAS*, 477, L117 (Paper I)
 Namouni, F. & Morais, M. H. M. 2020, *MNRAS*, 494, 2191 (Paper II)
 Nesvorný, D., Vokrouhlický, D., Stern, A. S., et al. 2019, *AJ*, 158, 132
 Rein, H. & Spiegel, D. S. 2015, *MNRAS*, 446, 1424
 Rein, H. & Tamayo, D. 2017, *MNRAS*, 467, 2377
 Rickman, H., Fouchard, M., Froeschlé, C., & Valsecchi, G. B. 2008, *Celestial Mechanics and Dynamical Astronomy*, 102, 111
 Tamayo, D., Rein, H., Shi, P., & Hernandez, D. M. 2020, *MNRAS*, 491, 2885
 Widmark, A. & Monari, G. 2019, *MNRAS*, 482, 262